# Millimeter-Wave Holographic Power Splitting/Combining

Mahmoud Shahabadi, *Member, IEEE,* and Klaus Schünemann, *Fellow, IEEE*

***Abstract*—It is shown that holography offers a novel solution to the problem of millimeter-wave power splitting and combining. With the help of an approximate model, we demonstrate that a hologram will work as a beam-splitting element, provided that it records the holographic image of the beams to be generated. To verify this observation, a beam splitter consisting of a hologram and an antenna array is analyzed by means of a rigorous network model. This analysis serves to find the optimum structure of the beam splitter. Measurements on a realized prototype of the beam splitter prove the possibility of achieving a high splitting efficiency, a high inter-element isolation, and a relatively large bandwidth. Flexibility in the orientation and the number of outputs is another outstanding feature of this holographic approach.**

***Index Terms*— Holographic power dividers/combiners, holographic recording, millimeter-wave power dividers/combiners, millimeter-wave technology.**

## I. Introduction

A SINGLE solid-state source for millimeter waves might hardly meet the requirements concerning the power level in many practical systems. This supports the idea of multi-element configurations for the purpose of power combining. The existing methods of power combining are assigned to two categories: *resonant* and *nonresonant* approaches [1]. In resonant methods, the sources coherently inject their energies into an eigenmode of a shielded [2], [3] or an open resonator [4]–[6] while nonresonant methods are mainly based on spatial combining of the energy radiated by an array of mutually locked oscillators [7]–[9]. To avoid mode competition in the former method and grating lobes in the latter method, the single sources should be arranged within a spacing dictated by the wavelength. (The distance between neighboring devices should typically be equal to or less than half a wavelength.) Therefore, at millimeter-wave frequencies, this requires a geometrically small inter-element spacing or, rather, circuit miniaturization. However, regarding the fact that solid-state millimeter-wave sources usually possess a low power efficiency, the individual sources should be equipped with heat sinks, which are as large as several wavelengths, so that electrical and thermal demands are normally in contradiction.

To overcome these shortcomings and to allow sufficient geometrical spacing between the output (input) ports, we have recently introduced a novel approach to power splitting (combining) by means of holography [10]. In this method, power splitting is performed by a *computer-generated* hologram storing holographic images of a given number of electromagnetic beams. Illumination of this hologram with an appropriate input beam reconstructs the stored images coherently. In other words, the introduced holographic method offers an elegant way for splitting a beam into a set of coherent beams and vice versa. Furthermore, since the recorded beams can arbitrarily be oriented in the hologram, the spacing between them may be chosen large enough to avoid the aforementioned problem of miniaturization.

This paper reports on the operation principles, design, and implementation of a millimeter-wave holographic power splitter/combiner. Firstly, with the aid of an approximate linear-system model, we discuss the operation principle of the power splitter/combiner in Section II. Section III is devoted to a rigorous analysis of a power splitter/combiner constituted by a phase grating and a horn array. Implementation of the power splitter/combiner along with the measurement results is described in Section IV.

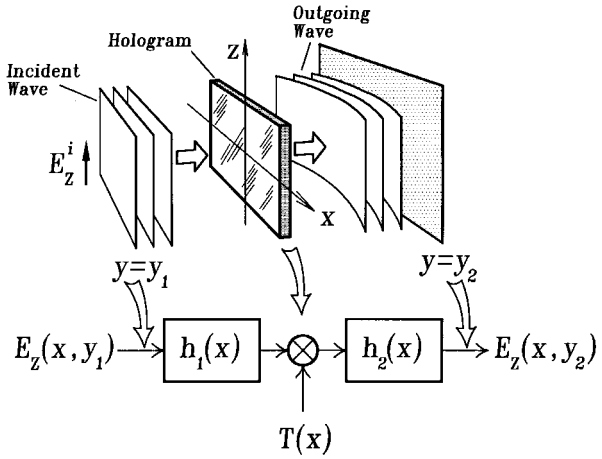


Fig. 1. Wavefront transformation with a hologram.

## II. Holography and Beam Splitting

This section deals with a simple optical model which provides an insight into the process of holographic beam splitting. To begin, consider the arrangement of Fig. 1, which shows an input wave incident on a hologram. While traversing the hologram, the incident wave undergoes a spatial amplitude and/or phase modulation. Although more or less any other optical element (e.g., a lens) also modulates its input

Manuscript received March 31, 1997; revised August 15, 1997. This work was supported by the Deutsche Forschungsgemeinschaft.

The authors are with Arbeitsbereich Hochfrequenztechnik, Technische Universität Hamburg-Harburg, D-21071 Hamburg, Germany.

Publisher Item Identifier S 0018-9480(97)08330-0.

wavefront, the modulation performed by a hologram relates to an interference pattern recorded in it, which renders the following distinguishing feature to this modulation. Assume that the recorded pattern is formed by two or more interfering wavefronts, and that it is stored in the transparency of the hologram in a way to be explained later. In the case that the input wave coincides with one of these waves, the wave leaving the hologram carries information about the other ones [11]–[13]. That is to say, the modulated wave can have some predetermined properties provided that the hologram records the *right* image. Let us see in a more quantitative manner how this image should look.

Looking at Fig. 1, suppose that the input wave is known in plane $y = y_1$, and that it should be transformed into a desired wave at plane $y = y_2$. To formulate this process, we are to follow the propagation of the input wave from plane $y = y_1$ to plane $y = y_2$. For the sake of simplicity, it is assumed that both the structure and the excitation are $z$-invariant, and that the input wave is $z$-polarized.

In the Cartesian coordinate system with $\mathbf{r} = (x, y)$, the input wave can be considered as the superposition of a finite or infinite number of plane waves (or space harmonics) [14] according to

$$E_z(x,y) = \frac{1}{2\pi}\int_{-\infty}^{+\infty} \tilde{E}_z(k_x) e^{-j\mathbf{k}\cdot\mathbf{r}}\, dk_x \tag{1}$$

where $\mathbf{k} = k_x\hat{\mathbf{x}} + k_y\hat{\mathbf{y}}$ determines the propagation direction of the plane wave $e^{-j\mathbf{k}\cdot\mathbf{r}}$, the amplitude of which is $\tilde{E}_z(k_x)\, dk_x/2\pi$. Since these plane waves should satisfy Maxwell's equations, either $k_x$ or $k_y$ may vary independently, while the other one is obtained from the relation $k_x^2 + k_y^2 = k_o^2$ (with $k_o$ as the free-space propagation constant). Knowing $E_z(x, y)$ in the plane $y = y_1$, and applying the inverse Fourier transformation along with the Sommerfeld radiation condition to (1), we can uniquely evaluate $\tilde{E}_z(k_x)$, i.e., the plane-wave (or spatial-frequency) spectrum of the input wave. Once this spectrum is known, the process of wave propagation will be completely described by (1).

When the input wave has a paraxial propagation along the $y$-axis, its spatial-frequency spectrum is mainly concentrated around $k_x = 0$, and relation (1) takes a simple form. This is due to the fact that for $|k_x| \ll k_o$, $k_y$ may be approximated by

$$k_y \approx k_o - \frac{1}{2}\frac{k_x^2}{k_o}. \tag{2}$$

Substituting (2) into (1) and expressing the field in the plane of the hologram $E_z(x, 0)$ in terms of the known field distribution $E_z(x, y_1)$, we obtain, after some straightforward steps, the following:

$$E_z(x,0) = \int_{-\infty}^{+\infty} h_1(x-x')E_z(x', y_1)\, dx' = h_1(x) * E_z(x, y_1) \tag{3}$$

with

$$h_1(x) = \left(\sqrt{\frac{j}{\lambda_o|y_1|}}e^{-jk_o|y_1|}\right)e^{-j\pi x^2/\lambda_o|y_1|}, \qquad k_o = \frac{2\pi}{\lambda_o}. \tag{4}$$

Based on (3), a *linear space-invariant* system with the impulse response $h_1(x)$ models the paraxial propagation of the input wave from the $y = y_1$ plane to the $y = 0$ plane. This has been shown in the block diagram of Fig. 1. It is worth mentioning that (3) might be interpreted as another expression for the Fresnel–Kirchhoff diffraction formula [15] in a form suitable for a linear-system representation. As previously mentioned, a hologram spatially modulates the wave incident on it. In Fig. 1, this effect is modeled by a multiplier. The function $T(x)$ in this model represents the amplitude *transparency* of the hologram at point $x$, so the field just behind it is obtained from the product $T(x)E(x, 0^-)$. If this field also satisfies the conditions of paraxiality, one is allowed to model its propagation from $y = 0$ to $y = y_2$ with another linear space-invariant system. The impulse response of this system, $h_2(x)$, can be derived from (4) after replacing $y_1$ by $y_2$. This completes the development of the required linear system for modeling the transformation done by the hologram.

Now we formulate the problem of beam splitting by finding a realizable function $T(x)$ for the transparency of the hologram so that a given input beam $E_z(x, y_1)$ will be transformed into a number of desired beams through the diffraction at the hologram.

Referring to the main characteristic of a hologram discussed at the beginning of this section, we expect that the solution to the above problem must be related to the interference pattern of the input and the desired beams. More precisely, since the beams to be generated specify $E_z(x, y_2)$ in the model of Fig. 1, the needed function $T(x)$ should satisfy

$$h_2(x) * (T(x) \cdot (h_1(x) * E_z(x, y_1))) = E_z(x, y_2) \tag{5}$$

which is an integral equation for the only unknown $T(x)$. However, the transparency function evaluated in this way is not always realizable. Even so, the solution of (5) does not necessarily lead to a lossless beam splitter. As a matter of fact, to synthesize a beam splitter of the highest possible efficiency, the magnitude of $T(x)$ should be unity since the systems corresponding to $h_1(x)$ and $h_2(x)$ are lossless. This justifies the necessity of a phase hologram for efficient beam splitting.

Another constraint on the function $T(x)$ is again derived from a case of practical interest, namely generation of a set of equidistant identical output beams from a uniform input beam. Such a set of beams requires the periodicity of $E_z(x, y_2)$. Hence, we deduce from (5) that the function $T(x)$ should also be periodic with the same period as that of $E_z(x, y_2)$.

On the other hand, to guarantee the realizability of the function $T(x)$ the design procedure can be based on the synthesis of a physical structure. To that end, a dielectric grating seems to be an optimum choice in view of its lossless transfer characteristic and the possibility to implement a periodic phase modulation. Thus, the next section is devoted to a rigorous analysis of a holographic beam splitter/combiner consisting of a dielectric grating.

## III. Rigorous Formulation

Fig. 2 illustrates the structure to be investigated. This two-dimensional (2-D) arrangement involves $A$, a horn array for

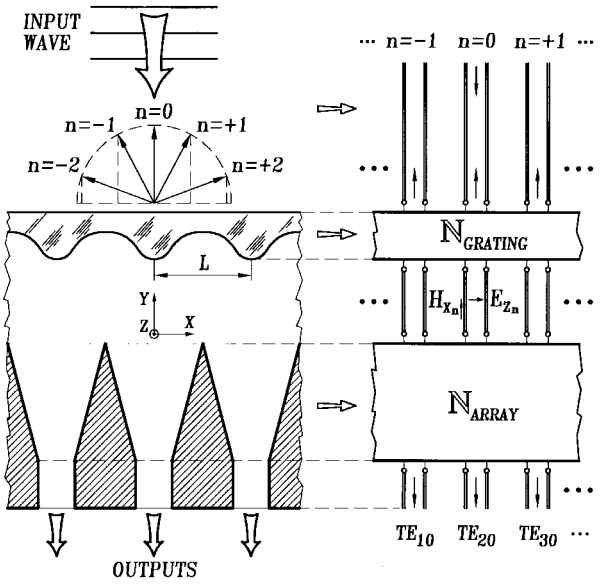


Fig. 2. A dielectric phase grating along with a horn array for collecting the output beams. An equivalent network of this structure is also seen in this figure. The arrows show the propagation direction of various space harmonics. Each transmission line in the equivalent network corresponds to one of the space harmonics.

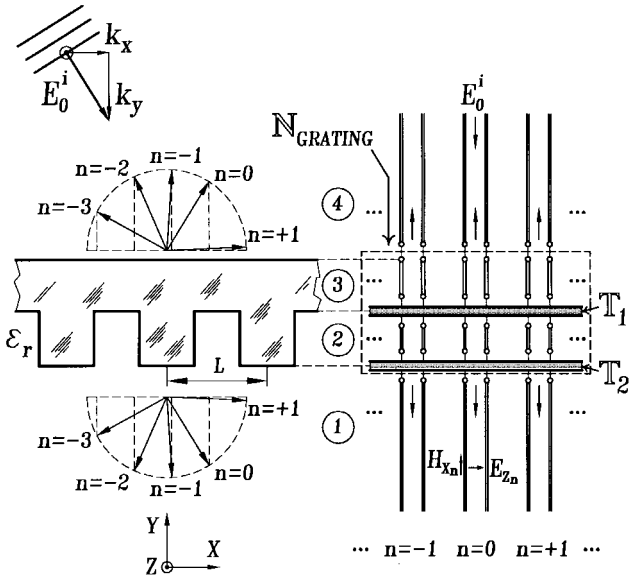


Fig. 3. Network model for a binary phase grating.

generation/collection of a number of electromagnetic beams, and $B$, a dielectric periodic structure operating as a phase hologram. Our goal is to find an optimum design for the grating so that the energy of a plane wave normal to the grating is entirely collected by the horn array in a manner that all of the horn antennas receive the same amount of power.

The periodic structure in Fig. 2 is a surface-relief grating with a simple mechanical construction in which the optical length and, consequently, the spatial phase shift varies as a function of groove height. In this case, the information recorded in the grating can be envisioned as the position-dependent phase shift caused by varying groove height. The same effect will be achieved if the refractive index of the dielectric grating changes from point to point.

To suffice the constraints explained in the last section, the period of the grating and that of the horn array are assumed equal. This period is predetermined and can amount to several wavelengths to allow for a large physical spacing among the array ports.

The analysis of the structure in Fig. 2 can be reduced to the analysis of an equivalent network when a plane wave excites this configuration. Because any general excitation can be expanded into a set of plane waves, the assumption of plane-wave excitation does not restrict the generality of this approach.

As far as the plane-wave excitation of the grating is concerned, all the components of the scattered field can be regarded as being pseudo-periodic functions.[1] Since the set of all space harmonics representing a pseudo-periodic function is denumerable, one could utilize an equivalent network of discrete transmission lines (like that seen in Fig. 2) to simulate the propagation of these space harmonics.

[1] A function $f(x)$ is called pseudo-periodic if there are some $L$ and $\alpha$ for which $f(x+L) = e^{-j\alpha L} f(x)$.

The multiport networks $\mathcal{N}_{\text{Array}}$ and $\mathcal{N}_{\text{Grating}}$ in Fig. 2 model the horn array and the grating, respectively. In the following subsections, we will investigate these networks in more detail.

### A. Hologram

In order to develop a network model for the hologram, we follow the approach proposed in [16]. The main steps of this method have been summarized in what follows.

Note that by approximating the groove shape of a surface-relief hologram with a staircase function, the hologram may be imagined as a stack of dielectric periodic structures having rectangular profiles. Thus, we first describe the network model for the rectangular periodic structure depicted in Fig. 3.

Inside region ② of Fig. 3, which we will call the periodic region, the relative permittivity varies periodically. As a consequence, we may uniquely expand the relative permittivity of this region as

$$\epsilon_r(x) = \lim_{N\to\infty} \sum_{n=-N}^{N} \tilde{\epsilon}_n \, e^{-j2n\pi x/L}. \tag{6}$$

To account for dielectric losses, complex values are assigned to the function $\epsilon_r(x)$. On the other hand, if the grating is excited by the plane wave $\hat{\mathbf{z}}E_0^i e^{-j(k_x x + k_y y)}$ with $k_y = -\sqrt{k_o^2 - k_x^2}$, the total field (i.e., the sum of the scattered and the incident field) will be pseudo-periodic. Thus, for the assumed incident polarization, the total field is a $\mathrm{TM}_z$ wave with the following tangential components:

$$E_z(x,y) = \lim_{N\to\infty} \sum_{n=-N}^{N} E_{Z_n}(y) e^{-j\alpha_n x} \tag{7}$$

$$H_x(x,y) = \lim_{N\to\infty} \sum_{n=-N}^{N} H_{X_n}(y) e^{-j\alpha_n x} \tag{8}$$

where $\alpha_n = k_x + 2n\pi x/L$. Substitution of (6)–(8) in Maxwell's equations leads to the succeeding matrix relation

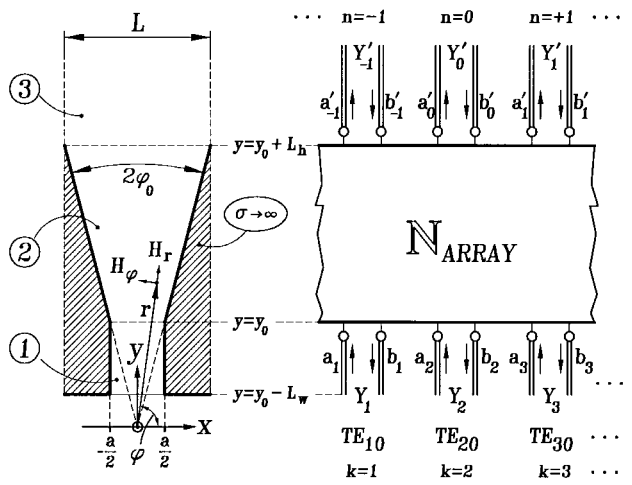


Fig. 4. Network model for the horn array.

for the unknown coefficients of (7) and (8):

$$\frac{d}{dy}\big[E_{Z_n}(y)\big] = -j\omega\mu_o\big[H_{X_n}(y)\big] \tag{9}$$

$$\frac{d}{dy}\big[H_{X_n}(y)\big] = -j\omega\epsilon_o[N]^2\big[E_{Z_n}(y)\big] \tag{10}$$

with

$$[N]^2 = \begin{pmatrix} & \cdots & & \\ & \left(\tilde{\epsilon}_o - \frac{\alpha_{-1}^2}{k_o^2}\right) & \tilde{\epsilon}_{-1} & \tilde{\epsilon}_{-2} & \\ \cdots & \tilde{\epsilon}_1 & \left(\tilde{\epsilon}_o - \frac{\alpha_0^2}{k_o^2}\right) & \tilde{\epsilon}_{-1} & \cdots \\ & \tilde{\epsilon}_2 & \tilde{\epsilon}_1 & \left(\tilde{\epsilon}_o - \frac{\alpha_1^2}{k_o^2}\right) & \\ & & \cdots & & \end{pmatrix} \tag{11}$$

and $k_o = \omega\sqrt{\mu_o\epsilon_o}$. As can be implied from (9) and (10), the coefficients of the space harmonics obey the laws of propagation along a multiconductor transmission line if $(E_{Z_n}, H_{X_n})$ is considered as the voltage–current pair of the $n$th transmission line. In the periodic region, these transmission lines are mutually coupled on account of the nondiagonal elements of $[N]^2$; while in a homogeneous region, like region ①,③, or ④ of Fig. 3, the matrix $[N]^2$ is diagonal, and the transmission lines are isolated from each other.

If the matrix $[N]^2$ is diagonalized (i.e., if one finds a diagonal matrix $[D]$ and a similarity transformation $[P]$ such that $[N]^2 = [P][D][P]^{-1}$), the transmission lines representing the periodic region will also be decoupled. Fig. 3 demonstrates the equivalent network of the hologram in its final form. Here the diagonalization procedure has been modeled by transformers $\mathcal{T}_1$ and $\mathcal{T}_2$, which correspond to $[P]$ and $[P]^{-1}$, respectively. Not to mention that the network model of any arbitrary surface-relief grating can be obtained by cascading the equivalent networks of the various layers appearing in the staircase approximation of the groove shape.

### *B. Horn Array*

Fig. 4 illustrates a single period of the horn array as well as a multiport network describing the energy exchange between the eigenmodes of the input waveguide and the space harmonics in region ③. The $\mathrm{TE}_y$ modes inside the waveguide, i.e., in region ①, contribute to the following tangential field components in the plane $y = y_0$:

$$E_z(y_0) = \lim_{K\to\infty}\sum_{k=1}^{K}(a_k + b_k)\sin\left(\frac{k\pi(x+a/2)}{a}\right) \tag{12}$$

$$H_x(y_0) = \lim_{K\to\infty}\sum_{k=1}^{K}Y_k(a_k - b_k)\sin\left(\frac{k\pi(x+a/2)}{a}\right) \tag{13}$$

where $a_k$ and $b_k$ represent the amplitude of the incident and reflected $\mathrm{TE}_{k,0}$ mode in the $y = y_0$ plane, respectively. $Y_k = k_{y_k}/\eta_o k_o$ with $\eta_o = \sqrt{\mu_o/\epsilon_o}$ and $k_{y_k}^2 = k_o^2 - (k\pi/a)^2$ is the admittance of the $\mathrm{TE}_{k,0}$ mode.

Inside the sectoral horn, the $E_z$-field component is expanded in terms of the Hankel functions of the first and second kind as

$$E_z = \sum_{\nu}\left(A_\nu H_\nu^{(2)}(k_o r) + B_\nu H_\nu^{(1)}(k_o r)\right) \times \sin\left(\nu\left(\varphi + \varphi_o - \frac{\pi}{2}\right)\right) \tag{14}$$

with $\nu = m\pi/2\varphi_o$, $m = 1, 2, \cdots, M \to \infty$. $A_\nu$ and $B_\nu$ are the unknown expansion coefficients to be determined. One may obtain the field components $H_r$ and $H_\varphi$ from (14) and Maxwell's equations, i.e.,

$$H_r = -\frac{1}{j\omega\mu_0}\frac{1}{r}\frac{\partial}{\partial\varphi}E_z \tag{15}$$

$$H_\varphi = \frac{1}{j\omega\mu_0}\frac{\partial}{\partial r}E_z. \tag{16}$$

The above field components are projected into the plane $y = y_0$ to yield the tangential magnetic field $H_x$:

$$H_x(x, y_0) = \frac{x}{\sqrt{x^2+y_0^2}}H_r - \frac{y_0}{\sqrt{x^2+y_0^2}}H_\varphi. \tag{17}$$

Suppose that the incident waves $[a_k]$ are given. Equating (12) to (14) and (13) to (17) for $|x| < a/2$ and $y = y_0$, we find[2] two infinite systems of equations for the three unknown vectors $[b_k]$, $[A_\nu]$, and $[B_\nu]$.

Two other infinite systems of equations may be obtained from the boundary conditions in the plane $y = y_0 + L_h$, i.e., in the aperture of the horn array. To that end, (14) and (17)—after replacing $y = y_0$ by $y = y_0 + L_h$—are used to specify the tangential field components in the plane $y = y_0 + L_h$. On the other hand, the most general form of the tangential field in region ③ just above the aperture reads

$$E_z(y_0 + L_h) = \lim_{N\to\infty}\sum_{n=-N}^{N}(a_n' + b_n')e^{-j2n\pi x/L} \tag{18}$$

$$H_x(y_0 + L_h) = \lim_{N\to\infty}\sum_{n=-N}^{N}Y_n'(a_n' - b_n')e^{-j2n\pi x/L} \tag{19}$$

where $a_n'$ and $b_n'$ denote the amplitude of the $n$th outgoing and incoming space harmonic, respectively. The admittance $Y_n'$ is given by $\sqrt{k_o^2 - (2n\pi/L)^2}/\eta_o k_o$ and equals the characteristic admittance of the transmission line corresponding to the $n$th

[2]To equate these equations, we equate their moments with respect to an appropriate set of weighting functions defined on $|x| < a/2$.

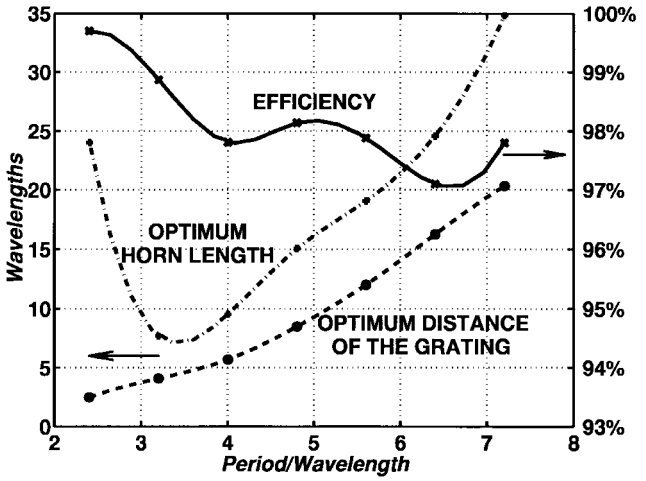


Fig. 5. Power-splitting efficiency for a rectangular grating as a function of the normalized period. Optimum grating distance and horn length are also seen in this diagram.

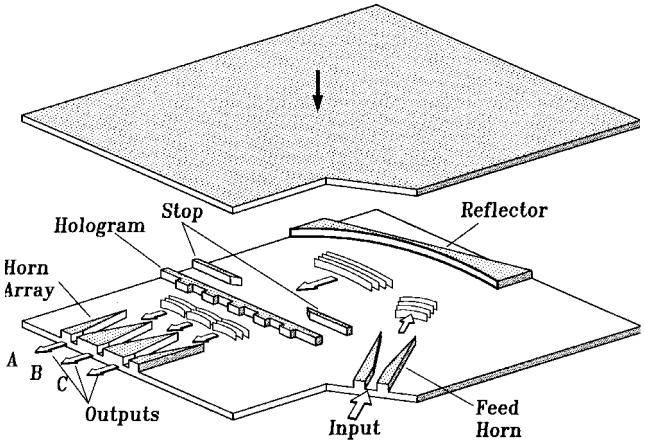


Fig. 6. Realization of a holographic beam splitter in parallel-plate technique.

space harmonic. By matching (18) and (19) to the aperture field of the horn, one arrives at the two needed infinite systems of equations for $[A_\nu]$, $[B_\nu]$, $[a'_n]$, and $[b'_n]$.

After elimination of $[A_\nu]$ and $[B_\nu]$ in the above four infinite systems of equations, the complete description of the network $\mathcal{N}_{\text{Array}}$ shows the following form:

$$\begin{pmatrix}[a_k]\\ [b_k]\end{pmatrix} = \begin{pmatrix}\mathcal{A} & \mathcal{B}\\ \mathcal{C} & \mathcal{D}\end{pmatrix}\begin{pmatrix}[a'_n]\\ [b'_n]\end{pmatrix}. \tag{20}$$

This is a chain or *ABCD* matrix representation for linking the eigenmodes of the input waveguide with the space harmonics in region ③.

Since the submatrices $\mathcal{A}$, $\mathcal{B}$, $\mathcal{C}$, and $\mathcal{D}$ have infinite dimensions, they should be truncated prior to any numerical computation. At this stage, the edge conditions for $y = y_0$ and $y = y_0 + L_h$ dictate the allowable $M/K$ and $N/M$ ratios in the truncated versions of (12)–(19).

### C. Design Procedure

In order to design a phase grating that efficiently transforms a normal incident plane wave into an array of electromagnetic beams, we investigate the reciprocal case. In other words, we excite the antennas of Fig. 2 uniformly, and attempt to maximize the power of the zeroth space harmonic. (Note that the zeroth space harmonic corresponds to a plane wave leaving the phase grating perpendicularly.) Thus, for a computer-aided design (CAD) of the beam splitter, we choose the energy of this space harmonic as object function. Later, in an iterative trial-and-error procedure, the parameters of the grating are varied according to an optimization strategy, until the energy of the zeroth space harmonic is maximized. Application of the equivalent network of the last two subsections facilitates the above design process considerably.

Regarding the fact that the spacing between the input ports (i.e., the period of the structure in Fig. 2) is predetermined, the optimum design of the beam splitter should be attained by varying the groove shape and the position of the phase grating as well as the length of the horn antennas. It has been found that the optimum groove shape tends to be rectangular. Typical values of the achieved power-splitting efficiency for a rectangular groove shape are shown in Fig. 5. As can be seen, the achieved efficiencies are higher than 97%, even for an inter-element spacing of several wavelengths, which is a proof for the scalability of this method up to very high frequencies of millimeter and submillimeter waves.

## IV. Implementation and Measurements

The introduced holographic approach has been implemented at 24 GHz in parallel-plate waveguide technique in accordance with the arrangement of Fig. 6. It consists of a dielectric phase grating as a hologram, a horn array for collecting the output beams, and a setup to generate a readout beam for reading the images recorded in the hologram. Owing to the propagation properties of the fundamental mode in a parallel-plate waveguide, the configuration of Fig. 6 exhibits the required characteristics for realizing the 2-D structure of Fig. 2.

The hologram has been designed with the help of the method discussed in the last section. Its period and, consequently, the spacing between adjacent outputs amounts to 80 mm $(= 6.4\lambda_o)$. It possesses a rectangular groove shape of 4.7-mm height, and is made out of Teflon, which shows relatively low losses at millimeter-wave frequencies. An ordinary milling machine has been utilized for fabricating the hologram.

To characterize the combination of the hologram and the horn array, we have measured the input scattering parameter $|S_{11}|$ for the center horn. (This measurement has been done in the absence of the reflector and the aperture stop to minimize the unwanted reflections.) In fact, the scattering parameter $|S_{11}|$ contains information not only about the diffraction at the grating, but also about the scattering centers of the horn, like its edges. Therefore, a comparison between the measured and simulated $|S_{11}|$ represents a valuable verification for the numerical simulation of Section III. The reflection $|S_{11}|$ and the mutual coupling between two neighboring horns $|S_{21}|$ measured with an HP 8510C network analyzer are seen in Figs. 7 and 8, respectively. These results not only verify our computation (dot–dashed curves), but also indicate a return loss of better than 15 dB and an isolation of higher than 25 dB

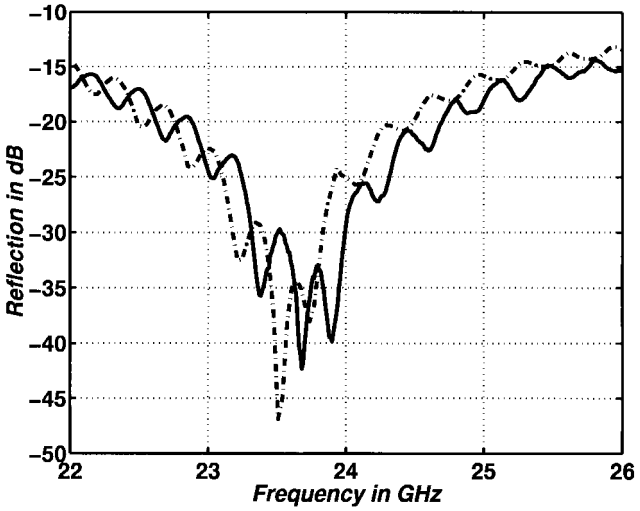


Fig. 7. Measured (—) and computed (−·) reflection.

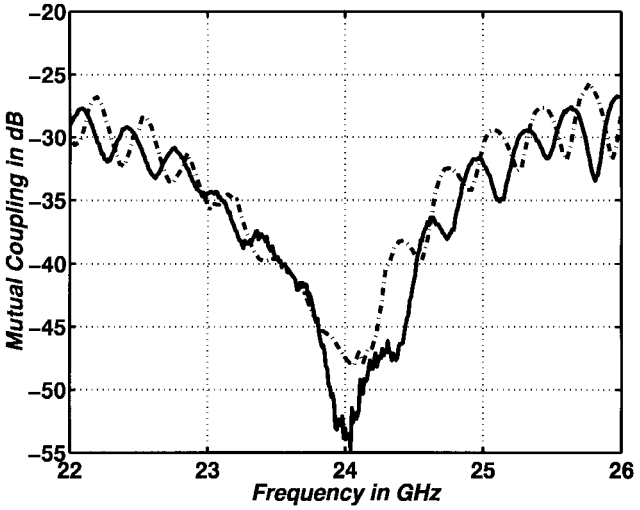


Fig. 8. Measured (—) and computed (−·) mutual coupling.

over a bandwidth of more than 15%. The slight deviation of the measured values from the simulated ones is probably caused by the ohmic losses on the walls of the horn antennas. The simulated electric-field distribution inside the beam splitter for the case where only the center horn is excited is shown in Fig. 9.

To generate a beam for reconstruction of the stored images in the hologram, the setup of Fig. 6 involves a feed horn, an offset reflector, and an aperture stop. The offset reflector having a length of $48\lambda_0$ is illuminated by the feed horn and provides a nearly Gaussian beam as shown in Fig. 10. This figure illustrates the measured field intensity at the position of the aperture stop when this and the other components are absent. The field intensity evaluated by using the method of moments is also shown in Fig. 10.

For an equi-power reconstruction of the recorded images, the hologram should be excited with a uniform (flat-top) beam. In Fig. 6, the $18\lambda_0$-wide aperture stop passes a portion of the Gaussian beam and flattens the field profile.

The normalized field intensity measured in a short distance behind the aperture stop as well as the simulation of the stop

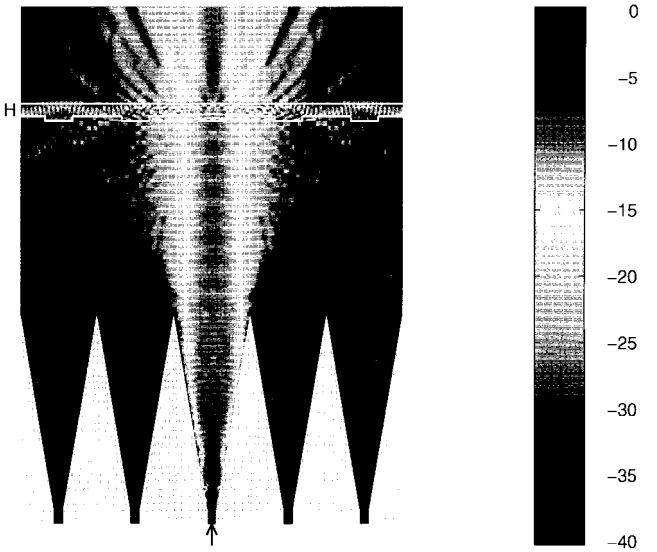


Fig. 9. Simulated field distribution inside the beam splitter. Only the middle horn is excited. The scale bar shows the magnitude of the electric field in decibels ($H$: Position of the hologram).

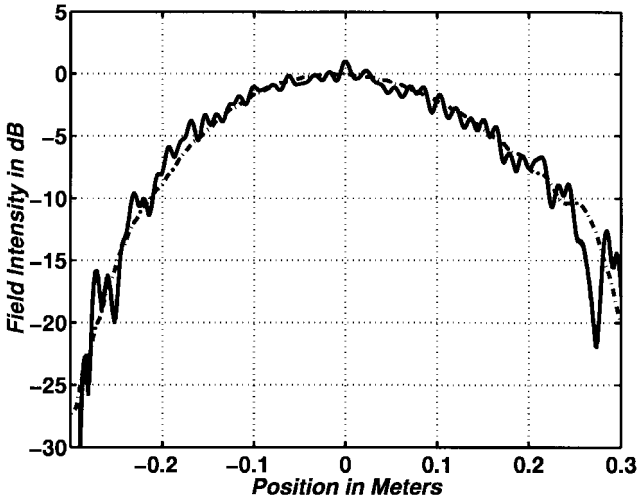


Fig. 10. Nearly Gaussian beam reflected from the reflector. Measured (—) and computed (−·).

by the method of moments are seen in Fig. 11. It should be noted that the applied procedure of beam equalizing is not an efficient one and shows an efficiency of only 70%. For a more efficient beam equalization, one can use lens-like refractive components [17], improve the feed system of the reflector, or modify the shape of the reflector [18].

Fig. 12 depicts the measured field intensity in the aperture of the horn array when the horn array is removed. It can clearly be seen that the hologram has recovered the recorded beams. Note the excellent agreement between the measured values and those computed by the method of Section III. See Fig. 13 for the simulated electric-field distribution in response to a Gaussian input beam. Three reconstructed beams and some higher diffraction orders are readily recognized in this figure.

The transmission characteristic between the feed horn and each output horn has been measured using an HP 8510C network analyzer. The result seen in Fig. 14 shows an overall

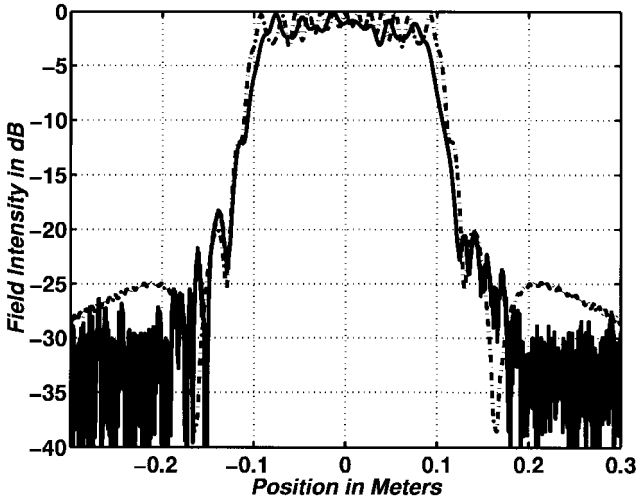


Fig. 11. Beam equalized by the aperture stop. Measured (—) and computed (−·).

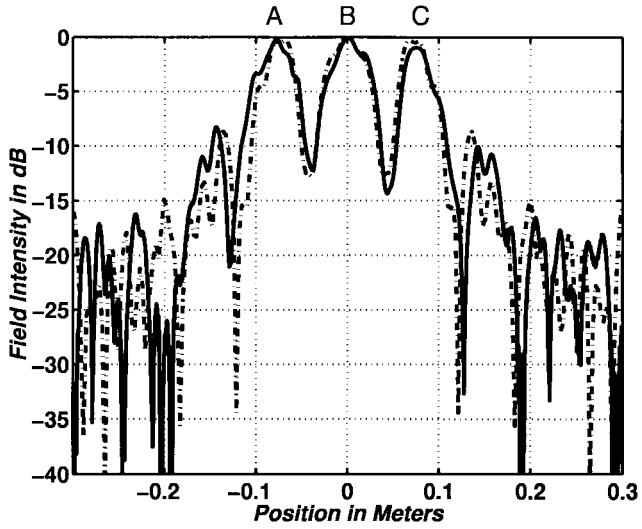


Fig. 12. Reconstruction of the three beams stored in the hologram. Measured (—) and computed (−·).

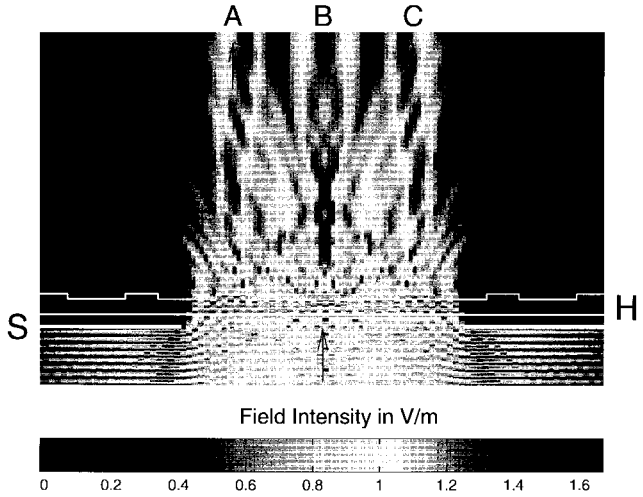


Fig. 13. Electric-field distribution in the vicinity of the hologram and the stop ($H$: Hologram. $S$: Stop. $A$, $B$, $C$: Output beams).

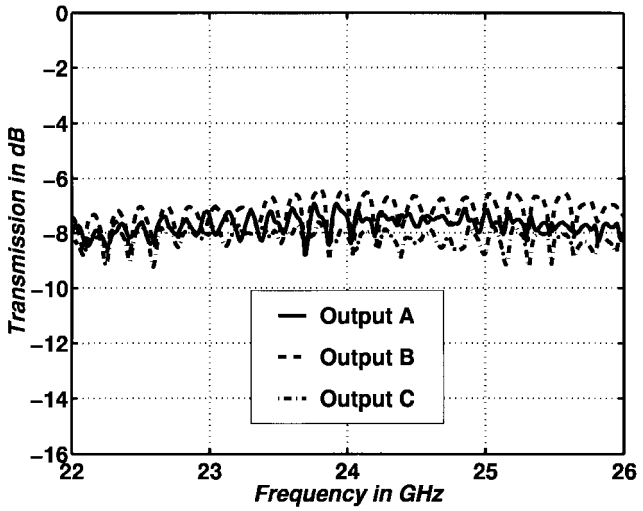


Fig. 14. Overall transmission characteristic for each output.

transmission of −8 ± 0.5 dB for all outputs. Owing to the limited efficiency of the beam-equalizing stop and regarding the ohmic losses in the parallel-plate waveguide, the measured power of the beam incident on the hologram is about 50% of the total input power, so an overall transmission of −8 ± 0.5 dB indicates that 93% of the power incident on the hologram has been received by the output horns. In the case where the hologram is removed, the power received by the array diminishes to only 25%.

The ripples observed in the frequency response of Fig. 14 are caused by multiple reflections between the reflector and the aperture stop, and will vanish by replacing the stop with a matched refractive beam equalizer like that proposed in [17].

## V. Comparison with Fraunhofer Holograms

A method comparable with the method of this paper is wavefront transformation by means of Fraunhofer holograms. In this section, we intend to point out the main differences between these two approaches.

As mentioned in Section II, the problem to be solved by the method of this paper is concerned with a wavefront transformation within the domain of Fresnel diffraction or equivalently in the near-field zone of a diffraction grating. The problem of wavefront transformation can also be posed for the far field. In this case, an incident wavefront should be transformed to a defined wavefront at infinity. This problem has gained attention in optics. To our knowledge, the early works by Lohmann [19] on the subject of wavefront reconstruction in the far-field zone of a binary hologram were the starting point for the development of other useful holographic optical elements for multiple imaging [20], [21] and beam addition [22], [23]. The basic element in all of these applications is a computer-generated hologram which transforms an incident plane wave into a number of equi-power space harmonics—known as Dammann grating. Evidently, a Dammann grating can be exploited as a beam splitter only in the far-field region. However, due to the fact that the period of a Dammann grating amounts to several wavelengths, at typical millimeter-wave frequencies the far-field region of this grating

exceeds several meters, so the above method is not practicable for millimeter waves unless additional optical components like Fourier transform lenses are added to its configuration [24]. In contrast to that, the method of this paper excludes any additional component and, therefore, maintains a very low splitting/combining loss.

Another notable advantage of a Fresnel beam-splitting hologram over its Fraunhofer counterpart is a higher achievable bandwidth. This may be justified by the reason that the propagation directions of the space harmonics produced by a Dammann grating obviously depend on the working frequency, which influences the coupling into the output ports and renders the transmission characteristic narrow-band.

Finally, note that the number of input/output ports for a Dammann grating cannot be changed without redesigning the grating, whereas this number in the introduced method is determined only by the number of periods.

## VI. Conclusion

A holographic power splitter/combiner has been presented in this paper. It is capable of becoming a favorite candidate for millimeter and submillimeter-wave applications because of its high efficiency, broad-band character, high isolation, and flexibility in both orientation and number of outputs.

## Acknowledgment

The authors are grateful to M. Akbari for his considerable assistance during these measurements.

## References

[1] K. Chang and C. Sun, "Millimeter-wave power-combining techniques," *IEEE Trans. Microwave Theory Tech.*, vol. MTT-31, pp. 91–107, Feb. 1983.

[2] K. Kurokawa and F. M. Magalhaes, "An $X$-band 10-watt multiple-IMPATT oscillator," *Proc. IEEE*, vol. 59, pp. 102–103, Jan. 1971.

[3] K. Chang, W. F. Thrower, and G. M. Hayashibara, "Millimeter-wave silicon IMPATT sources and combiners for the 110–260-GHz range," *IEEE Trans. Microwave Theory Tech.*, vol. MTT-29, pp. 1278–1284, Dec. 1981.

[4] L. Wandinger and V. Nalbandian, "Millimeter-wave power combiner using quasi-optical techniques," *IEEE Trans. Microwave Theory Tech.*, vol. MTT-31, pp. 189–193, Feb. 1983.

[5] J. W. Mink, "Quasi-optical power combining of solid-state millimeter-wave sources," *IEEE Trans. Microwave Theory Tech.*, vol. MTT-34, pp. 273–279, Feb. 1986.

[6] J. Bae, Y. Aurakawa, H. Kondo, T. Tanaka, and K. Mizuno, "Millimeter and submillimeter wave quasioptical oscillator with Gunn diodes," *IEEE Trans. Microwave Theory Tech.*, vol. MTT-41, pp. 1851–1855, Oct. 1993.

[7] K. D. Stephan, "Inter-injection-locked oscillators for power combining and phased arrays," *IEEE Trans. Microwave Theory Tech.*, vol. MTT-34, pp. 1017–1025, Oct. 1986.

[8] Z. B. Popovic and D. B. Rutledge, "Diode-grid oscillators," in *IEEE Antennas Propagation Symp. Dig.*, Syracuse, NY, 1988, pp. 442–445.

[9] R. A. York and R. C. Compton, "Quasi-optical power combining using mutually synchronized oscillator arrays," *IEEE Trans. Microwave Theory Tech.*, vol. 39, pp. 1000–1009, June 1991.

[10] M. Shahabadi and K. Schünemann, "Holographic power combining: A new principle for millimeter and submillimeter-wave power combining," in *Proc. 26th European Microwave Conf.*, Prague, Czech Republic, Sept. 9–12, 1996, pp. 115–119.

[11] D. Gabor, "Holography, 1948–1971," *Proc. IEEE*, vol. 60, pp. 655–668, June 1972.

[12] J. W. Goodman, "An introduction to the principles and applications of holography," *Proc. IEEE*, vol. 59, pp. 1292–1304, Sept. 1971.

[13] H. M. Smith, *Principles of Holography*, 2nd ed. New York: Wiley, 1975.

[14] R. F. Harrington, *Time-Harmonic Electromagnetic Fields*. New York: McGraw-Hill, 1961 ch. 4.

[15] M. Born and E. Wolf, *Principles of Optics*, 6th ed. New York: Pergamon, 1983.

[16] M. Shahabadi, K. Schünemann, and H.-G. Unger, "Modeling of diffraction at dielectric biperiodic objects using an equivalent network," in *Dig. 20th Int. Conf. Infrared Millimeter Waves*, Orlando, FL, Dec. 11–14, 1995, pp. 397–398.

[17] J. L. Kreuzer, "Coherent light optical system yielding an output beam of desired intensity distribution at a desired equiphase surface," U.S. Patent 3 476 463, Nov. 1969.

[18] D.-W. Duan and Y. Rahmat-Samii, "A generalized diffraction synthesis technique for high performance reflector antennas," *IEEE Trans. Antennas Propagat.*, vol. 43, pp. 27–40, Jan. 1995.

[19] A. W. Lohmann and D. P. Paris, "Binary Fraunhofer holograms, generated by computer," *Appl. Opt.*, vol. 6, pp. 1739–1748, Oct. 1967.

[20] S. Lu, "Generating multiple images for integrated circuits by Fourier-transform holograms," *Proc. IEEE*, vol. 56, pp. 116–117, Jan. 1968.

[21] H. Dammann and K. Görtler, "High-efficiency in-line multiple imaging by means of multiple phase hologram," *Opt. Commun.*, vol. 3, pp. 312–315, July 1971.

[22] J. R. Leger, G. J. Swanson, and W. B. Veldkamp, "Coherent beam addition of GaAlAs lasers by binary phase gratings," *Appl. Phys. Lett.*, vol. 48, pp. 888–890, Apr. 1986.

[23] J. R. Leger, G. J. Swanson, and W. B. Veldkamp, "Coherent laser addition using binary phase gratings," *Appl. Opt.*, vol. 26, pp. 4391–4399, Oct. 1987.

[24] J. A. Murphy, S. Withington, and M. Heanue, "Local oscillator splitting using Dammann phase gratings," presented at the *3rd Int. Workshop Terahertz Electron.*, Zermatt, Switzerland, Aug. 31–Sept. 1, 1995.

**Mahmoud Shahabadi** (S'88–M'90) was born in Tehran, Iran, in 1966. He received the B.Sc. and M.Sc. degrees in electrical engineering from the University of Tehran, Tehran, Iran, in 1988 and 1991, respectively, and is currently working toward the Ph.D. degree in electrical engineering at the Technische Universität Hamburg-Harburg, Hamburg, Germany. His current research field involves millimeter-wave quasi-optical techniques and the application of holography to millimeter-wave systems.

Mr. Shahabadi was awarded the Deutscher Akademischer Austauschdienst (DAAD) Scholarship in 1992.

**Klaus Schünemann** (M'76–SM'86–F'95) was born in Braunschweig, Germany, in 1939. He received the Dipl.-Ing. degree in electrical engineering and the Doktor-Ing. degree from the Technische Universität Braunschweig, Braunschweig, Germany, in 1965 and 1969, respectively.

Since 1983, he has been a Professor of electrical engineering and Director of the Arbeitsbereich Hochfrequenztechnik at the Technische Universität Hamburg-Harburg, Hamburg, Germany. He has worked on nonlinear microwave circuits, diode modeling, solid-state oscillators, PCM communication systems, and integrated-circuit technologies such as finline and waveguide-below-cutoff. His current research interests are concerned with transport phenomena in submicron devices, CAD of planar millimeter-wave circuits, optoelectronics, high-power and high-frequency tubes, submillimeter-wave circuit technology, and millimeter- and submillimeter-wave radars for climate and environmental research.